RSC Advances

PAPER

View Article Online
View Journal | View Issue

Cite this: *RSC Adv.*, 2018, **8**, 9822

Linear-type carbazoledioxazine-based organic semiconductors: the effect of backbone planarity on the molecular orientation and charge transport properties†

Rikuo Otsuka, Yang Wang, * Takehiko Mori and Tsuyoshi Michinobu *

Received 3rd February 2018
Accepted 27th February 2018

DOI: 10.1039/c8ra01088a

rsc.li/rsc-advances

We report the synthesis of a linear-type dibromocarbazoledioxazine (**CZ**) derivative as a new precursor for semiconducting polymers. The chemical structures of the **CZ** unit and its polymers with thiophene or thienothiophene spacers (namely, **PCZT** and **PCZTT**) were fully characterized. **PCZT** and **PCZTT** possessed similar medium optical band gap (E_g^{opt}) and electrochemical band gap (E_g^{cv}) of around 1.70 eV estimated from the onset absorption and electrochemical redox potentials of the thin films, respectively. Computational density functional theory (DFT) calculations suggested that the backbone of the **PCZT** might be highly twisted, while that of **PCZTT** could be very planar. The effect of different backbone geometries on the charge–transport properties was studied by using thin film transistors (TFTs). The TFT device based on **PCZTT** showed a four times higher hole mobility as compared to that based on **PCZT**. The superior TFT performances of **PCZTT** were reasonably attributed to its edge-on backbone packing orientations toward the Si substrate revealed by the grazing-incidence wide-angle X-ray scattering (GIWAXS), which was favorable for in-plane charge transport in the TFT devices.

Introduction

With their interesting optical and electrical properties, organic semiconductors are increasingly prominent in various electronic devices such as organic photovoltaics (OPVs)[1–9] and organic thin film transistors (TFTs).[10–18] In particular, due to their solution processability and mechanical flexibility, organic semiconductors would become fundamental components for novel mobile electronic devices, such as flexible displays, biocompatible sensors, and radio frequency identification (RFID) tags.[19–21] In order to realize such next-generation devices, significant efforts have been devoted to the development of new organic semiconducting materials, some of which already demonstrated charge carrier mobilities beyond the benchmark of industry standard inorganic materials, such as amorphous silicon (0.1–1 $cm^2\ V^{-1}\ s^{-1}$).[22–25] One important strategy of designing the organic/polymeric semiconducting materials is to envision more promising building blocks.[26–28] While the electron-donating building blocks have been intensively explored,[29–31] the development of acceptor units lags behind because of the limited species and synthetic difficulties.[32] Among the reported acceptor building blocks, dye/pigment molecules have received enormous interests. Diketopyrrolopyrrole (DPP),[33] isoindigo (IID),[34] and rylene diimide (such as naphthalenediimide (NDI) and perylenediimide (PDI))[35–37] (Chart 1 top) are successful examples for the construction of high-performance semiconducting polymers with mobilities (μ) > 1 $cm^2\ V^{-1}\ s^{-1}$ in organic TFTs and power conversion efficiencies (PCE) > 10% in OPVs.[38]

Among these dye/pigment molecules, the angular-type carbazoledioxazine (**CZ**, X = Cl, Chart 1 middle), also called pigment violet 23, is a well-known commercial pigment, but it has been less explored in the field of organic electronics.[39–42] Note that this pigment is not only a member of the electron-accepting dioxazine family, but also originates from the electron-donating carbazole.[43,44] Thus, the violet color is derived from the highly-efficient intramolecular charge-transfer (CT) band. The general synthesis of this pigment is based on the condensation of a 3-aminocarbazole derivative with *p*-chloranil followed by two-fold cyclization reactions. In the final cyclization process, simple heating selectively affords the angular-type **CZ** (Chart 1 middle). On the other hand, the introduction of the methoxy-substituent into the 2-position of the carbazole unit produces the linear-type **CZ** under the same conditions (Chart 1 middle).[45,46] The electrochemical and optical properties of some **CZ** derivatives were investigated in the 1990s.[47,48] However, there have been, to the best of our knowledge, no reports about their applications in organic electronic devices until our recent

Department of Materials Science and Engineering, Tokyo Institute of Technology, 2-12-1 Ookayama, Meguro-ku, Tokyo 152-8552, Japan. E-mail: wang.y.av@m.titech.ac.jp; michinobu.t.aa@m.titech.ac.jp; Fax: +81-3-5734-3774; Tel: +81-3-5734-3774

† Electronic supplementary information (ESI) available: ^{1}H NMR spectra of the monomer and oligomers, TGA and DSC curves, current–voltage (*I–V*) characteristics of TFT devices. See DOI: 10.1039/c8ra01088a

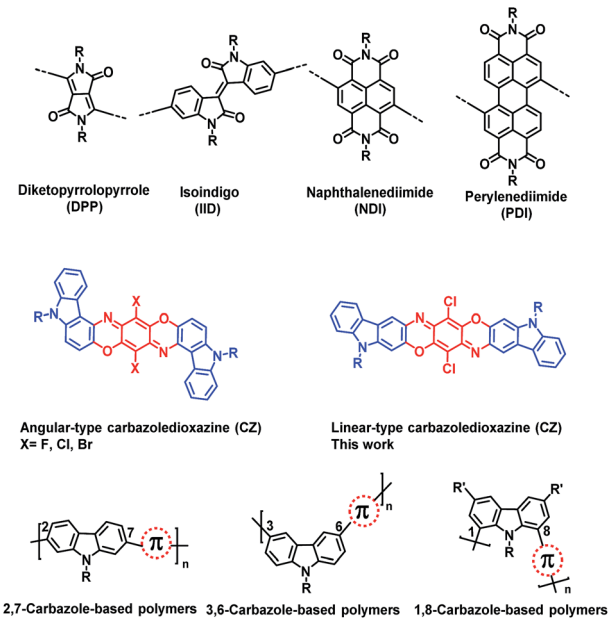

Chart 1 Chemical structures of (top) well-known dye/pigment units used for high-performance semiconducting polymers; (middle) angular and linear-type carbazoledioxazines; (bottom) 2,7-carbazole-, 3,6-carbazole-, and 1,8-carbazole-based copolymers.

publication of the first TFTs based on newly-designed angular-type CZs with different halogen atoms (Chart 1 middle, X = F, Cl, Br).[49] The TFT studies suggested that the **CZ** derivatives are relatively good *p*-type semiconductors with hole mobilities as high as 4.9×10^{-3} cm^2 V^{-1} s^{-1}. However, to the best of our knowledge, no studies have been reported so far for the synthesis of carbazoledioxazine-based polymers. Therefore, we became interested in incorporating the **CZ** unit into semiconducting polymers to further explore intriguing optical and electronic properties.

In view of the historical development of carbazole-based semiconducting polymers, the **CZ** molecular backbone shape was carefully designed. The linear-type 2,7-carbazole was previously shown to be a backbone component of semiconducting polymers superior to the angular-type 3,6-carbazole and 1,8-carbazole connectivities (Chart 1 bottom),[50–57] although 1,8-carbazole-based copolymers recently found a promising application possibility as fluorescent polymer nanoparticles (Pdots).[58,59] For instance, Leclerc *et al.* reported a 2,7-carbazole-based copolymer, namely poly(*N*-9-heptadecanyl)-2,7-carbazole-alt-5,5-(4,7-di-2-thienyl-2,1,3-benzothiadiazole) (PCDTBT), which demonstrated an excellent TFT mobility and OPV performances.[51–53] We anticipated that the angular- and linear-type CZs are analogous to these carbazole connectivities. Therefore, we decided to adopt the linear-type **CZ** structure in this study, rather than the recently reported angular-type **CZ** unit. The linear-type dibromo-**CZ** was thus newly designed and synthesized *via* a multistep synthesis (Scheme 1). This bifunctional monomer was then reacted with ditin–thiophene or ditin–thienothiophene units by Stille polycondensation, producing two promising semiconductors, namely **PCZT** and **PCZTT**, respectively (Scheme 1). The frontier energy levels (highest occupied molecular orbital: HOMO; lowest unoccupied molecular orbital: LUMO) and band gaps of **CZ** and its polymers were determined by their optical and electrochemical properties. Most importantly, the backbone planarity was estimated from the computational calculations. There was a clear correlation between these physical properties and TFT performances. The TFTs based on **PCZTT** displayed a hole mobility as high as 1.8×10^{-3} cm^2 V^{-1} s^{-1}, which was four times higher than that based on **PCZT**. This difference in the TFT performances was mainly attributed to the different backbone planarity, which was reasonably supported by their different solid-state packing structures and thin-film morphologies revealed by their X-ray diffraction measurements and atomic force microscopy images.

Experimental

General measurements

Nuclear magnetic resonance (NMR) spectra were recorded using a JEOL model AL300 (300 MHz) at room temperature. Deuterated chloroform was used as the solvent. Chemical shifts of NMR were reported in ppm (parts per million) relative to the residual solvent peak at 7.26 ppm for ^{1}H NMR spectroscopy and 77.6 ppm for ^{13}C NMR spectroscopy. Coupling constants (*J*) were given in Hz. The resonance multiplicity was described as s (singlet), d (doublet), t (triplet), and m (multiplet). Fourier transform infrared (FT-IR) spectra were recorded on a JASCO FT/IR-4100 spectrometer in the range from 4000 to 600 cm^{-1}. MALDI-TOF mass spectra of small molecules were measured on a Shimadzu/Kratos AXIMACFR mass spectrometer equipped with a nitrogen laser (λ = 337 nm) and pulsed ion extraction, which was operated in a linear-positive ion mode at an accelerating potential of 20 kV. Tetrahydrofuran (THF) solutions containing 1 g L^{-1} of a sample, 20 g L^{-1} of dithranol, and 1 g L^{-1} of sodium trifluoroacetate were mixed at a ratio of 1 : 1 : 1; and then 1 μL aliquot of this mixture was deposited onto a sample target plate. MALDI-TOF mass spectra of polymers were measured on a Bruker UltrafleXtreme mass spectrometer, which was operated in a linear-positive ion mode. Dithranol was used as a matrix. Elemental analysis was conducted at the Center for Advanced Materials Analysis, Tokyo Institute of Technology. The elements of C, H, and N were measured on a J-Science JM10, the elements of Cl, Br, and S on a Yanako HSU-20+ICS-1100, and the element of O on an Elementar Vario micro cube. UV-vis-NIR spectra were recorded on a JASCO V-670 spectrophotometer. Thermogravimetric analysis (TGA) and differential scanning calorimetry (DSC) measurements were carried out on a Rigaku TG8120 and a Rigaku DSC8230, respectively, under nitrogen flow at the scan rate of 10 °C min^{-1}. Electrochemistry measurements were carried out on a BAS electrochemical analyzer model 612C at 20 °C in a classical three-electrode cell. The working, reference, and auxiliary electrodes were a glassy carbon electrode, Ag/$AgNO_3$/CH_3CN/(nC_4H_9)$_4NPF_6$, and a Pt wire, respectively. For calibration, the redox potential of ferrocene/ferrocenium (Fc/Fc^+) was measured. It was assumed that the redox potential of Fc/Fc^+ has an absolute energy level of −4.80 eV to vacuum. The HOMO and LUMO

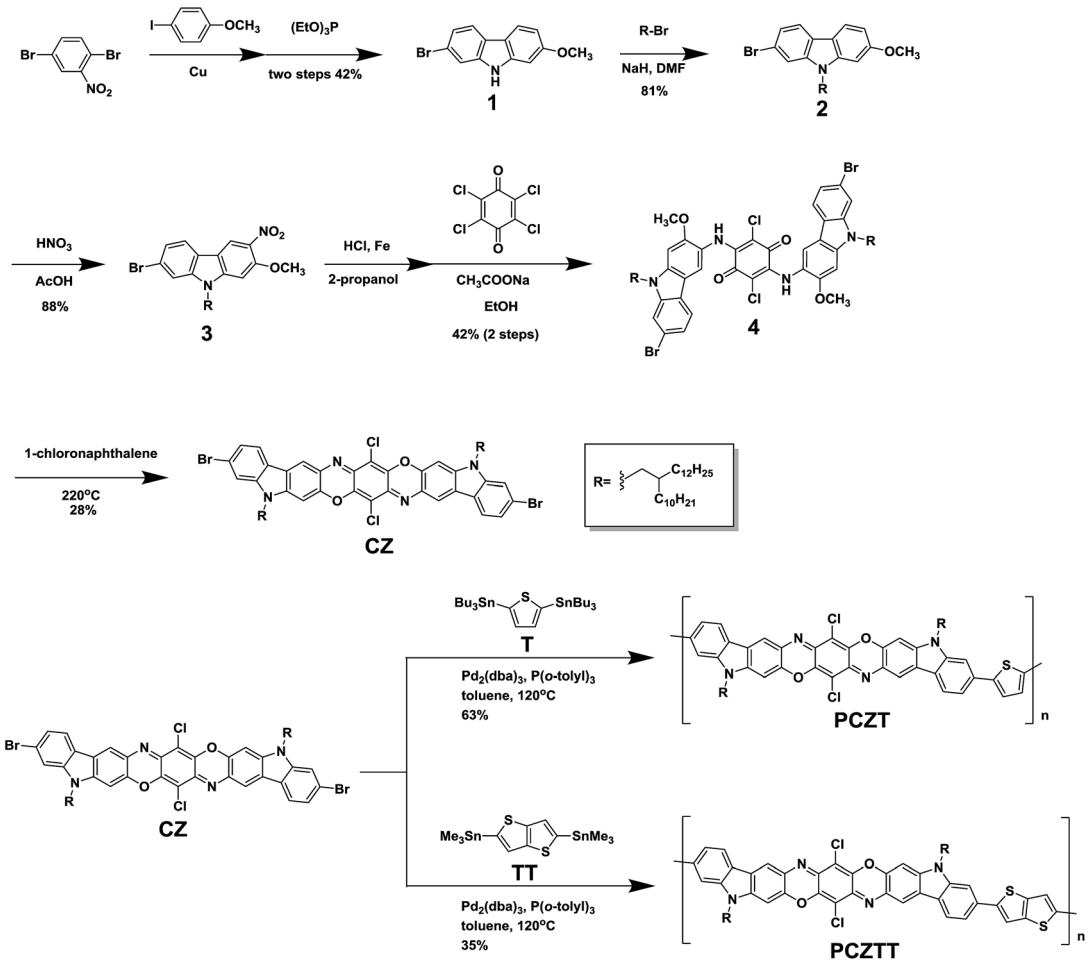

Scheme 1 Synthesis of the linear-type dibromocarbazoledioxazine monomer and its Stille polycondensation to give the corresponding semiconducting oligomers.

energy levels were then calculated according to the following equations:

$$E_{HOMO} = -(\varphi_{ox} + \varphi_{Fc/Fc^+} + 4.80)\ (eV) \quad (1)$$

$$E_{LUMO} = -(\varphi_{re} + \varphi_{Fc/Fc^+} + 4.80)\ (eV) \quad (2)$$

where φ_{ox} is the onset oxidation potential *vs.* $Ag/AgNO_3$, φ_{re} is the onset reduction potential *vs.* $Ag/AgNO_3$, and φ_{Fc/Fc^+} is the redox potential of ferrocene/ferrocenium *vs.* $Ag/AgNO_3$ and it is -0.05 V in this study.

Fabrication and characterization of thin film transistors

Top-contact/bottom-gate TFT devices were fabricated using n^+-Si/SiO_2 substrates where n^+-Si and SiO_2 were used as the gate electrode and gate dielectric, respectively. The substrates were subjected to cleaning with deionized water, acetone, and 2-propanol. Then, the substrates were cleaned with O_3 for 20 min using a Technovision model 208 UV-O_3 cleaning system. The cleaned substrates were modified with octadecyltrimethoxysilane (OTMS) to form a self-assembled monolayer (SAM). Thin films of the **CZ**-based semiconductors were deposited on the treated substrate by spin-coating a chloroform solution (5 g L^{-1}), followed by thermal annealing at 150, 200, 250, or 300 °C for 10 min in an argon-filled glove box. After the thin film deposition, ~50 nm thick gold was deposited as source and drain contacts using a shadow mask. The TFT devices had a channel length (L) of 100 μm and a channel width (W) of 1 mm. The TFT performances were measured under ambient conditions using a Keithley 4200 parameter analyzer on a probe stage. The carrier mobilities, μ, were calculated from the data in the saturated regime according to the following equation:

$$I_{SD} = (W/2L)C_i\mu(V_{GS} - V_{th})^2 \quad (3)$$

where I_{SD} is the drain current in the saturated regime, W and L are the semiconductor channel width and length, respectively, C_i ($C_i = 13.3$ nF cm^{-2}) is the capacitance per unit area of the gate dielectric layer, and V_{GS} and V_{th} are the gate voltage and threshold voltage, respectively. $V_{GS} - V_{th}$ of the devices was determined from the square root values of I_{SD} at the saturated regime. Current on/off ratios (I_{on}/I_{off}) were determined from the minimum current at around $V_{GS} = +20$ to -20 V (I_{off}) and the current at $V_{GS} = -80$ V (I_{on}). The transfer characteristics were obtained by sweeping the V_{GS} from +20 to -80 V.

Grazing-incidence wide angle X-ray scattering (GIWAXS) measurements

The GIWAXS profiles were obtained by using a Phillips X'Pert-Pro-MRD with monochromated CuKα radiation (wavelength = 0.154 nm) operated at 45 kV and 40 mA in air. The samples were exposed to the X-ray beam for 1 h with an incident beam radius of 320 mm. The thin films for GIWAXS were prepared by spin-coating the polymer solutions on OTMS-treated Si/SiO_2 substrates followed by thermal annealing at the optimized temperature for 10 min under vacuum.

Atomic force microscopy (AFM) measurements

AFM samples were prepared by spin-coating the polymer solutions on OTMS-treated Si/SiO_2 substrates. Both pristine and thermally-treated films were examined by a Seiko Instruments SPA-400 with a stiff cantilever of Seiko Instruments DF-20.

Materials and synthetic details

All chemicals were purchased from Tokyo Chemical Industry (TCI), Kanto Chemical, and Sigma Aldrich and used as received unless otherwise stated. 2-Bromo-7-methoxy-9*H*-carbazole **1** and 11-(bromomethyl)tricosane were prepared according to a literature method.[49,60]

Synthesis of 2-bromo-9-(2-decyltetradecyl)-7-methoxy-9*H*-carbazole (2)

NaH (2.50 g, 60% dispersion in paraffin liquid) in dry DMF (80.0 mL) was slowly added to 2-bromo-7-methoxy-9*H*-carbazole (4.34 g, 15.7 mmol) under nitrogen. After stirring for 30 min, 11-(bromomethyl)tricosane (7.83 g, 20.8 mmol) was added and the mixture was stirred at room temperature for 1 day. The reaction mixture was quenched with H_2O and extracted with CH_2Cl_2. Evaporation followed by column chromatography (SiO_2, hexane/CH_2Cl_2 4 : 1) afforded the desired compound as colorless oil (7.83 g, 81%).

^{1}H NMR (300 MHz, $CDCl_3$): δ = 7.92 (d, J = 8.4 Hz, 1H), 7.84 (d, J = 8.4 Hz, 1H), 7.47 (d, J = 1.5 Hz, 1H), 7.30 (dd, J = 8.6, 1.3 Hz, 1H), 6.88 (dd, J = 8.6, 2.0 Hz, 1H), 6.82 (d, J = 2.2 Hz, 1H), 4.06 (d, J = 7.7 Hz, 2H), 3.94 (s, 3H), 2.10 (br, 1H), 1.23 (m, 40H), 0.90 (t, J = 6.6 Hz, 6H) ppm; ^{13}C NMR (75 MHz, $CDCl_3$): δ = 159.18, 142.38, 141.90, 121.89, 121.86, 120.94, 120.43, 117.75, 116.18, 111.75, 107.49, 93.63, 55.56, 47.66, 37.54, 31.92, 31.90, 31.73, 29.92, 29.66, 29.65, 29.60, 29.56, 29.37, 29.32, 29.49, 22.68, 14.12 ppm; IR (neat): ν = 2922, 2852, 1634, 1597, 1519, 1457, 1334, 1309, 1247, 1063, 825, 811, 718 cm^{-1}; MALDI-TOF MS (M_w = 612.8): m/z = 612.6 [M$^+$].

Synthesis of 7-bromo-9-(2-decyltetradecyl)-2-methoxy-3-nitro-9*H*-carbazole (3)

To a solution of **2** (5.34 g, 8.71 mmol) in acetic acid (80 mL), a mixture of fuming nitric acid (2.0 mL, 48.2 mmol) and acetic acid (100 mL) was dropwise added at room temperature for over 30 min. After saturated aqueous solution of sodium bicarbonate was added, the organic phase was extracted with CH_2Cl_2. Evaporation followed by column chromatography (SiO_2, hexane/CH_2Cl_2 1 : 1) afforded the desired compound as yellow oil (5.02 g, 88%).

^{1}H NMR (300 MHz, $CDCl_3$): δ = 8.54 (s, 2H), 7.80 (d, J = 8.1 Hz, 2H), 7.71 (s, 2H), 7.48 (d, J = 1.5 Hz, 2H), 7.32 (dd, J = 8.2, 1.6 Hz, 2H), 6.80 (s, 2H), 4.08 (d, J = 7.3 Hz, 4H), 3.98 (s, 6H), 2.10 (br, 2H), 1.22 (m, 80H), 0.87 (t, J = 6.6 Hz, 12H) ppm; ^{13}C NMR (75 MHz, $CDCl_3$): δ = 153.71, 144.50, 142.80, 133.61, 123.88, 121.72, 121.35, 119.84, 119.60, 114.97, 112.82, 92.77, 56.84, 48.09, 37.71, 32.04, 32.01, 31.87, 30.08, 29.98, 29.82, 29.78, 29.75, 29.71, 29.66, 29.59, 29.54, 29.47, 29.43, 26.74, 26.62, 22.92, 22.86, 22.82, 14.36, 14.24 ppm; IR (neat): ν = 2922, 2852, 1634, 1597, 1519, 1457, 1334, 1308, 1247, 1063, 1028, 825, 811, 720 cm^{-1}; MALDI-TOF MS (M_w = 657.8): m/z = 657.9 [M$^+$].

Synthesis of 2,5-bis((7-bromo-9-(2-decyltetradecyl)-2-methoxy-9*H*-carbazol-3-yl)amino)-3,6-dichlorocyclohexa-2,5-diene-1,4-dione (4)

Iron dust (22.5 g, 0.403 mol) was added to water (30 mL) and aqueous HCl (10 N, 5 mL), and the mixture was stirred at 90 °C for 30 min under nitrogen. After a solution of **3** (8.64 g, 13.1 mmol) in 2-propanol (150 mL) was added, the mixture was refluxed for 5 h. After cooling to room temperature, water was added and the organic phase was extracted with CH_2Cl_2. Evaporation yielded 7-bromo-9-(2-decyltetradecyl)-2-methoxy-9*H*-carbazol-3-amine, and this compound was subjected to the next reaction without further purification. *p*-Chloranil (1.64 g, 6.67 mmol), sodium acetate (0.542 g, 6.61 mmol), and ethanol (200 mL) were added, and the mixture was refluxed under nitrogen for 5 h. After cooling to room temperature, water was added and the organic phase was extracted with CH_2Cl_2. Evaporation followed by column chromatography (SiO_2, hexane/CH_2Cl_2 5 : 4) afforded the desired compound as a reddish-purple solid (3.95 g, two-step yield of 42%).

^{1}H NMR (300 MHz, $CDCl_3$): δ = 8.07 (s, 2H), 7.77 (d, J = 8.0 Hz, 2H), 7.32 (dd, J = 8.1, 1.6 Hz, 2H), 7.48 (d, J = 1.5 Hz, 2H), 7.32 (dd, J = 8.2, 1.6 Hz, 2H), 6.80 (s, 2H), 4.08 (d, J = 7.3 Hz, 4H), 3.98 (s, 6H), 2.10 (br, 2H), 1.22 (m, 80H), 0.87 (t, J = 6.6 Hz, 12H) ppm; ^{13}C NMR (75 MHz, $CDCl_3$): δ = 173.74, 153.56, 142.98, 141.99, 140.78, 122.59, 121.84, 120.90, 119.24, 118.46, 118.35, 114.42, 112.24, 102.71, 91.37, 56.09, 48.02, 37.84, 32.06, 32.02, 31.95, 30.50, 29.82, 29.79, 29.77, 29.73, 29.71, 29.49, 29.45, 26.66, 22.83, 14.25 ppm; IR (neat): ν = 3226, 2925, 2853, 1738, 1714, 1574, 1465, 1363, 1219, 755, 745 cm^{-1}; MALDI-TOF MS (M_w = 1428.5): m/z = 1429.2 [M$^+$].

Synthesis of 3,13-dibromo-8,18-dichloro-5,15-bis(2-decyltetradecyl)-5,15-dihydrocarbazolo[3′,2′:5,6][1,4]oxazino[2,3-*b*]indolo[2,3-*i*]phenoxazine (CZ)

A solution of **4** (0.442 g, 0.309 mmol) in 1-chloronaphthalene (8.0 mL) was heated to 220 °C for 26 h under nitrogen. After cooling to room temperature, the mixture was poured into methanol. The precipitate was collected by filtration and further purified by Soxhlet extraction with acetone for 24 h and the residue was finally extracted with chloroform. Further purification was performed by recycling preparative HPLC to yield the desired product as a violet solid (0.124 g, 28%).

^{1}H NMR (300 MHz, $CDCl_3$): δ = 8.07 (s, 2H), 7.77 (d, J = 8.0 Hz, 2H), 7.32 (dd, J = 8.1, 1.6 Hz, 2H), 7.20 (d, J = 1.4 Hz, 2H), 6.82 (s, 2H), 3.75 (d, J = 7.3 Hz, 4H), 1.95 (br, 2H), 1.24 (m, 80H), 0.88 (t, J = 6.6 Hz, 12H) ppm; ^{13}C NMR (75 MHz, $CDCl_3$): δ = 143.19, 142.82, 142.24, 142.18, 141.65, 128.82, 122.98, 121.39, 121.13, 121.12, 120.40, 119.66, 112.52, 109.89, 94.90, 48.23, 37.63, 32.08, 31.83, 30.14, 29.86, 29.84, 29.81, 29.54, 29.50, 26.62, 22.84, 14.27 ppm; MALDI-TOF MS (M_w = 1360.4): m/z = 1361.4 $[M + H]^+$.

Synthesis of PCZT

CZ (204 mg, 0.150 mmol), 2,5-bis(tributylstannyl)thiophene (99.1 mg, 0.150 mmol), $Pd_2(dba)_3$ (6.0 mg, 6.6 μmol), and P(*o*-tolyl)$_3$ (4.9 mg, 16 μmol) in toluene (15 mL) were refluxed for 2 days under nitrogen. After cooling to room temperature, the reaction mixture was poured into methanol (400 mL). The precipitate was collected by filtration and purified by Soxhlet extraction using methanol, acetone, hexane, and chloroform in this order. The chloroform soluble fraction was concentrated and reprecipitated into methanol, yielding a dark blue solid (193 mg, 63%).

GPC (eluent: *o*-dichlorobenzene): M_n = 6.2 kg mol^{-1}, PDI = 2.5; ^{1}H NMR ($CDCl_3$, 300 MHz): δ = 8.01–5.50 (br, 12H), 5.02–3.10 (br, 4H), 2.00–0.60 (br, 47H) ppm; IR (neat): ν = 3068, 3018, 1574, 1457, 1434, 1219, 1127, 1036, 942, 772, 748, 660 cm^{-1}; anal. calcd for $(C_{82}H_{110}Cl_2N_4O_2S)_n$: C, 76.54; H, 8.62; Cl, 5.51; N, 4.35; O, 2.49; S, 2.49; found: C, 73.41; H, 7.92; Br, 1.74; Cl, 5.32; N, 3.98; O, 4.35; S, 2.62.

Synthesis of PCZTT

CZ (244 mg, 0.179 mmol), 2,5-bis(trimethylstannyl)thieno[3,2-*b*]thiophene (81.9 mg, 0.179 mmol), $Pd_2(dba)_3$ (8.9 mg, 9.7 μmol), and P(*o*-tolyl)$_3$ (5.3 mg, 17 μmol) in toluene (20 mL) was refluxed for 2 days under nitrogen. After cooling to room temperature, the reaction mixture was poured into methanol (400 mL). The precipitate was collected by filtration and purified with Soxhlet extraction using methanol, acetone, hexane, and chloroform in this order. The chloroform soluble fraction was concentrated and reprecipitated into methanol, yielding a dark blue solid (85.0 mg, 35%).

GPC (eluent: *o*-dichlorobenzene): M_n = 6.8 kg mol^{-1}, PDI = 2.3; ^{1}H NMR ($CDCl_3$, 300 MHz): δ = 8.47–5.90 (br, 12H), 4.75–3.50 (br, 4H), 2.47–0.62 (br, 47H) ppm; IR (neat): ν = 2923, 2852, 1635, 1607, 1554, 1457, 1353, 1312, 1271, 1220, 1171, 1128, 1022, 906, 772 cm^{-1}; anal. calcd for $(C_{84}H_{110}Cl_2N_4O_2S_2)_n$: C, 75.13; H, 8.26; Cl, 5.28; N, 4.17; O, 2.38; S, 4.77; found: C, 72.95; H, 8.09; Br, 2.87; Cl, 4.96; N, 3.96; O, 3.37; S, 4.16.

Results and discussion

Synthesis and characterization

Starting from the commercially-available 1,4-dibromo-2-nitrobenzene, 2-bromo-7-methoxy-9*H*-carbazole (**1**) was obtained in the moderate yield of 42% in two steps according to a literature report.[60] Alkylation at the 9-position followed by mono-nitration yielded 7-bromo-9-(2-decyltetradecyl)-2-methoxy-3-nitro-9*H*-carbazole (**3**) in high yield (two steps, total yield over 70%, Scheme 1). The reduction of **3** by hydrochloric acid and Fe powder afforded the corresponding 3-amino-carbazole derivative, and this compound was directly used for the next condensation reaction with *p*-chloranil (2,3,5,6-tetrachlorocyclohexa-2,5-diene-1,4-dione) due to the limited stability of amine compound in air. The resulting product (**4**) was further subjected to a ring closure reaction at high temperature (220 °C) in 1-chloronaphthalene as the solvent, leading to the target linear carbazoledioxazine monomer (**CZ**) in 28% isolated yield after multiple purifications by Soxhlet extraction and recycling preparative high performance liquid chromatography (HPLC). The chemical structure of the new bifunctional monomer was unambiguously characterized by ^{1}H-, ^{13}C-NMR, IR spectroscopies and MALDI-TOF mass spectrometry. Particular attention was paid to the isomeric structures of this product. The resonance multiplicity of a set of aromatic proton peaks was observed as a singlet (protons d and g in Fig. 1 or protons a and b in Fig. S1†), clearly suggesting the formation of the linear-type structure. This was also consistent with the reported spectral patterns of similar derivatives.[45–48] In addition, after ring closure, the proton peaks of N–H and OCH_3 as well as the IR peaks ascribed to the C=O and NH vibrations completely disappeared (Fig. 1 and S2†).

The linear-type dibromocarbazoledioxazine monomer (**CZ**) was then reacted with the ditin compounds of thiophene (**T**) and thienothiophene (**TT**) by the conventional Stille polycondensation to afford the target products, namely **PCZT** and **PCZTT**, respectively (Scheme 1). They were washed using a Soxhlet extractor with the sequence of methanol, hexane, and acetone to remove the low molecular weight oligomers. Finally, the chloroform soluble fractions were collected and were found to be reasonably soluble in a variety of chlorinated solvents, such as chloroform, chlorobenzene, and 1,2-dichlorobenzene at room temperature. Thus, the molecular weights (number-average molecular weight (M_n) and weight-average molecular weight (M_w)) were determined by gel permeation chromatography (GPC) measurements using polystyrene as the standard and 1,2-dichlorobenzene as the eluent at 40 °C. Both polymers showed similar molecular weights and polydispersity indices

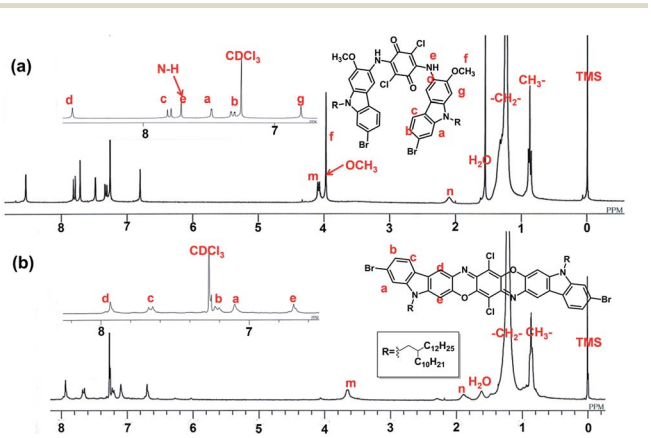

Fig. 1 ^{1}H NMR spectra of (a) **4** and (b) **CZ** in $CDCl_3$.

(PDI, M_w/M_n): **PCZT** (M_n = 6.2 kg mol^{-1}, M_w = 15.5 kg mol^{-1}, PDI = 2.5) and **PCZTT** (M_n = 6.8 kg mol^{-1}, M_w = 15.4 kg mol^{-1}, PDI = 2.3). The M_n values of **PCZT** and **PCZTT** suggested the pentamers (Table 1 and Fig. S3†). This was also supported by the comprehensive elemental analysis of both polymers. Importantly, a small amount of Br was detected (1.74% for **PCZT** and 2.87% for **PCZTT**). Under the assumption that the both terminal units are Br–**CZ**, the M_n was calculated to be 9.1 kg mol^{-1} for **PCZT** and 5.5 kg mol^{-1} for **PCZTT**, which were consistent with the GPC results. These results also suggested that the rate-determining step of the Stille polycondensation is oxidative addition. Note that we very recently developed a highly efficient Stille polycondensation protocol,[61] but this protocol was not applied to this study in order to avoid the side reaction at the Cl moieties of **CZ**. Interpretation of the conjugated polymer structures by NMR is often difficult due to the significant peak broadening caused by strong intermolecular interactions and wide molecular weight distributions. In particular, in the case of **PCZT** and **PCZTT**, the **CZ** monomer possesses two kinds of halogen moieties, namely, Br and Cl. In order to confirm the selective reaction at the Br moieties, MALDI-TOF mass spectrometry was used as an additional tool for structure verification. As shown in Fig. 2, one could observe some sets of molecular ion peaks ascribed to the desired repeat unit structures. These spectra support the progress of the Stille polycondensation at the Br moieties of the **CZ** monomer and rule out the possibility of undesired side reactions at the Cl moieties. It should be noted that the peak intensities of the MALDI-TOF mass spectra significantly decrease as the molecular weights increase, although they are dependent on the sample purity, molecular weight distributions, and matrix and instrument settings.

Thermal properties

The thermal stability of the polymers was estimated by thermogravimetric analysis (TGA) under a nitrogen atmosphere at the heating rate of 10 °C min^{-1} (Fig. S4†). Both **PCZT** and **PCZTT** exhibited a similar thermal stability profile with the 5% weight loss temperatures (T_d) being ~365 °C (365 °C for **PCZT** and 368 °C for **PCZTT**). The T_d values were sufficiently high for advanced studies of the TFT fabrication, which requires optimization of the thermal annealing conditions. The thermal transition properties were also investigated by differential scanning calorimetry (DSC) measurements in the temperature range without thermal decomposition under N_2 at the heating or cooling rate of 10 °C min^{-1} (Fig. S5†). Although no sharp transitions appeared, both polymers showed some endothermic

Table 1 Molecular weights, optical and electrochemical properties of the CZ monomer and its polymers

	M_n[a] (g mol^{-1})	PDI[a]	DP[a]	λ_{sol} (nm)	λ_{film}[b] (nm)	λ_{onset} (nm)	E_g^{optc} (eV)	φ_{ox}[d] (V)	φ_{re}[d] (eV)	E_{HOMO} (eV)	E_{LUMO} (eV)	E_g^{CV} (eV)
CZ	1364.4	—	—	554, 599	573, 629	702	1.77	0.52	−1.25	−5.27	−3.50	1.77
PCZT	6200	2.5	5	389, 620	399, 663	744	1.67	0.42	−1.28	−5.17	−3.47	1.70
PCZTT	6800	2.3	5	412, 624	433, 677	770	1.61	0.35	−1.29	−5.10	−3.46	1.64

[a] Determined by GPC. [b] Cast onto the glass substrate. [c] Optical band gap (E_g^{opt}) estimated from the onset wavelength of the films. [d] Thin films measured in CH_3CN with 0.1 M $(nC_4H_9)_4NClO_4$ at the scan rate of 0.1 V s^{-1}. Potentials *vs.* Fc/Fc$^+$.

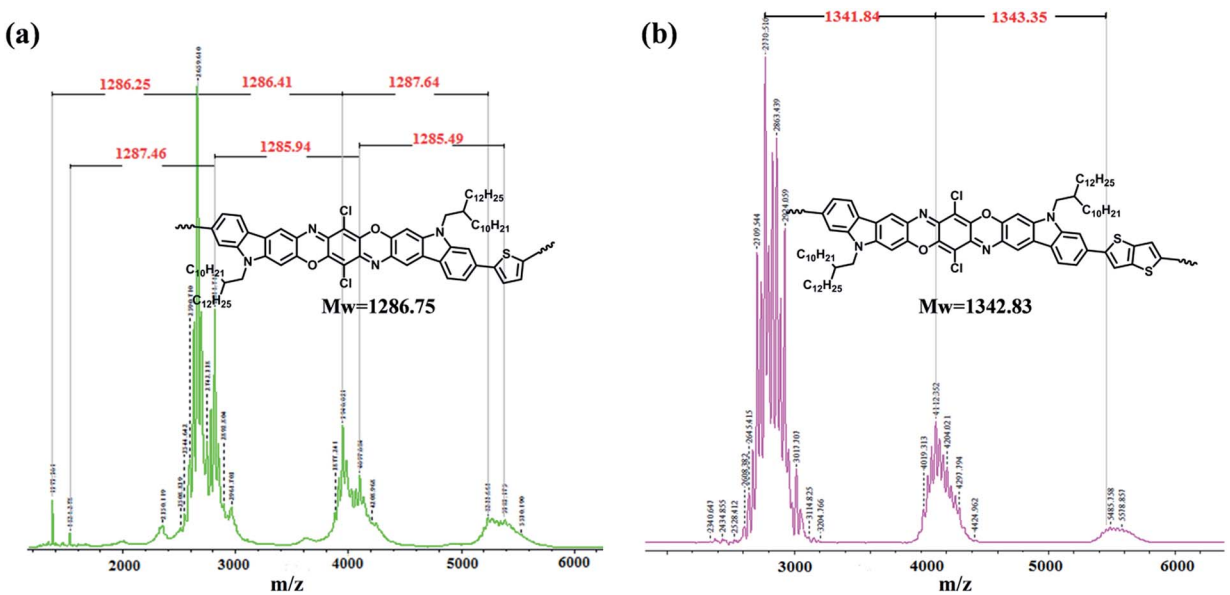

Fig. 2 MALDI-TOF mass spectra of (a) **PCZT** and (b) **PCZTT**.

and exothermic peaks during the heating and cooling processes, respectively. For example, **PCZT** displayed a transition at 208 °C in the second heating process, suggesting the existence of some different phases. **PCZTT** also showed a similar phase behavior.[14,15]

Optical and electrochemical properties

The absorption spectra of **CZ**, **PCZT**, and **PCZTT** in both solutions and thin films are shown in Fig. 3a. **CZ** displayed two absorption peaks with an optical band gap (E_g^{opt}) of 1.77 eV estimated from the onset wavelength (λ_{onset}) of the film (Table 1). After reacting with the thiophene or thienothiophene comonomer units, **PCZT** and **PCZTT** further extended the effective conjugation length, leading to red-shifted absorption with a narrower band gap of 1.67 and 1.61 eV, respectively.[13] The absorption maxima in dilute 1,2-dichlorobenzene solution and in the thin film state (λ_{sol} and λ_{film}) of **PCZTT** bathochromically shifted as compared to those of **PCZT**. For example, the film absorption (λ_{film}) of **PCZTT** was detected at 433 and 677 nm, while the **PCZT** film showed the λ_{film} of 399 and 663 nm (Table 1). Accordingly, **PCZTT** possessed a longer λ_{onset} and narrower E_g^{opt} than **PCZT**. This superior optical property of **PCZTT** was reasonably attributed to the stronger electron-donating nature of the thienothiophene unit, which elongates the effective conjugation length and raises the HOMO level.[4,13]

To determine the frontier energy levels, cyclic voltammograms (CVs) were measured as shown in Fig. 3b and the corresponding data are listed in Table 1. Thin films of the samples were prepared on a glassy carbon electrode, and their CVs were measured in CH_3CN with 0.1 M $(nC_4H_9)_4NClO_4$ at room temperature under an argon atmosphere.[13] All three samples displayed a well-defined reversible oxidation peak and an irreversible reduction one. The oxidation currents were much higher than the corresponding reduction ones (Fig. 3b), indicating the more facilitated hole injection to these thin films.[11,12] The highest occupied molecular orbital (E_{HOMO}) and lowest unoccupied molecular orbital (E_{LUMO}) values were estimated from the onset oxidation (φ_{ox}) and onset reduction (φ_{re}) potentials, respectively. As listed in Table 1, the monomer **CZ** possessed the E_{HOMO}/E_{LUMO} of −5.27/−3.50 eV, which were comparable to its angular type counterparts.[49] The thin film of **PCZT** showed the φ_{ox} of 0.42 V and φ_{re} of −1.28 V, corresponding to the E_{HOMO} value of −5.17 eV and the E_{LUMO} value of −3.47 eV. The frontier energy levels of **PCZTT** were similarly determined. While the HOMO level of **PCZTT** was 0.07 eV higher than that of **PCZT**, the LUMO levels of both polymers were almost the same within experimental error (merely 0.01 eV). The electrochemical band gaps (E_g^{CV}) of both polymers, calculated from the φ_{ox} and φ_{re} values, correlated with their E_g^{opt} (Table 1). For example, the E_g^{CV} values of both polymers were 0.03 eV higher than the corresponding E_g^{opt}.[13]

In order to further understand the optoelectronic properties and molecular geometry of the new polymers, density functional theory (DFT) calculations were performed using the

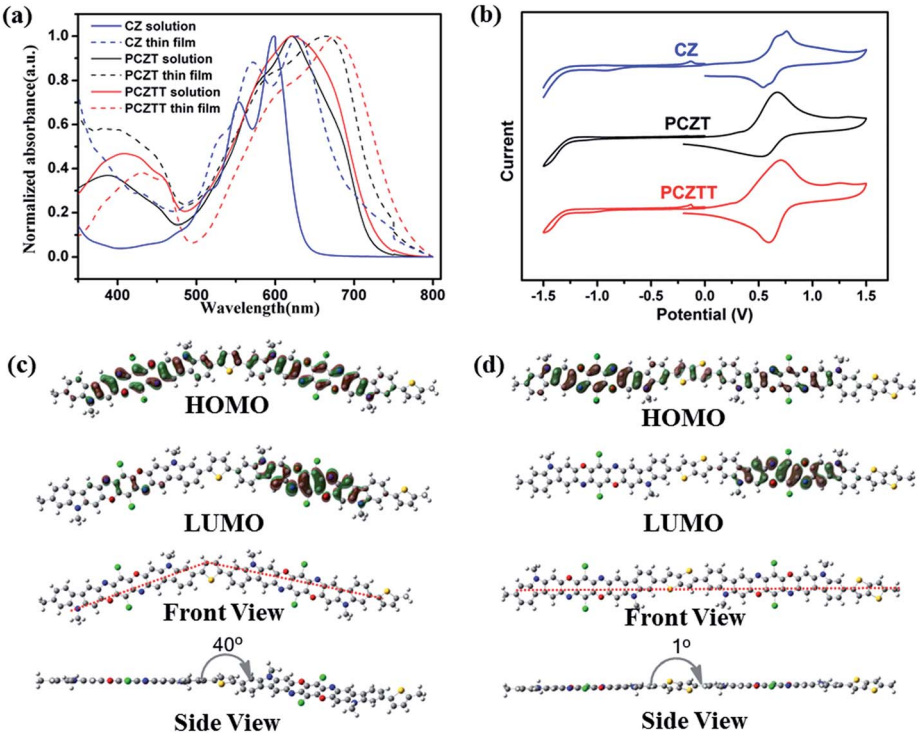

Fig. 3 (a) UV-vis-NIR absorption profiles of **CZ**, **PCZT**, and **PCZTT** in dilute 1,2-dichlorobenzene solution and thin film states spin-cast on a glass substrate; (b) cyclic voltammograms of the **CZ**, **PCZT**, and **PCZTT** films drop-cast on a glassy carbon electrode, measured in acetonitrile with 0.1 M $(nC_4H_9)_4NClO_4$ at the scan rate of 0.1 V s^{-1}; (c) calculated HOMO/LUMO orbitals and side-view geometry of **PCZT**; and (d) calculated HOMO/LUMO orbitals and side-view geometry of **PCZTT** (using DFT B3LYP/6-31G(d), long and branched alkyl chains are substituted by the methyl group).

dimer structures as the models with a B3LYP/6-31G(d) basis set.[22] The *N*-alkyl substituents and alkyl side chains were simplified as a methyl group. The molecular orbitals (MOs) and side-view geometry are shown in Fig. 3c and d. One could observe that the HOMO orbitals were well distributed along the backbone, while the LUMO orbitals were located on one side (mainly on the acceptor units). This kind of HOMO/LUMO distribution well explains the CV results. The radical cations formed through the one-electron oxidation are stable due to the delocalization of the HOMO orbitals. On the other hand, the chemical stability of the radical anions formed through a one-electron reduction is limited due to the localized LUMO on the acceptor unit.[13] Interestingly, there was an explicit difference in the optimized backbone geometry between **PCZT** and **PCZTT**. The **PCZT** dimer formed an angular-shape causing a twisted backbone with the dihedral angle of 40°. In contrast, the **PCZTT** dimer possessed an almost planar backbone due to the negligible steric repulsion between the adjacent repeat units (Fig. 3c and d bottom). These calculations are consistent with the experimental optical and electrochemical results.

Fabrication and measurements of thin film transistors

To further study the different backbone geometries effect on the charge transport properties, organic TFTs with bottom-gate/top-contact structures were fabricated by spin-coating the polymer solutions onto an octadecyltrimethoxysilane (OTMS)-treated SiO_2 (300 nm)/n^+-Si substrate.[13,22] After thermal annealing at some selected temperatures (100, 150, 250, or 300 °C), ~50 nm thick gold was deposited as the source and drain contacts using a shadow mask. As anticipated from the determined shallow HOMO (*ca.* −5.1 eV) and LUMO (*ca.* −3.5 eV) levels, both polymers showed unipolar p-type transistor performances (Fig. 4a to d). For example, the as-cast films of **PCZT** and **PCZTT** exhibited hole mobilities (μ_h) of 1.4×10^{-4} and 5.1×10^{-5} $cm^2\ V^{-1}\ s^{-1}$, respectively (Fig. 4a and c and Table 2). Subsequently, we tried thermal annealing to optimize the TFT performances. Unexpectedly, the mobility of **PCZT** decreased to 3.5×10^{-5} $cm^2\ V^{-1}\ s^{-1}$ after the thermal annealing at 100–150 °C, but it recovered to 1.4×10^{-4} $cm^2\ V^{-1}\ s^{-1}$ when the thermal annealing temperature was raised to 250 °C (Fig. 4e and Table 2). The highest μ_h of 3.0×10^{-4} $cm^2\ V^{-1}\ s^{-1}$ was achieved after thermal annealing at 300 °C (Fig. 4b and e and Table 2). On the other hand, the mobility of **PCZTT** had a linear correlation with the thermal annealing temperature (Fig. 4e). The highest μ_h of 1.4×10^{-3} $cm^2\ V^{-1}\ s^{-1}$ was achieved with the annealing temperature of 300 °C (Fig. 4d). It should be noted that this value is relatively good, considering the amorphous thin film structures of these polymers (for the GIWAXS results, *vide infra*).[11,12,57,62] Overall, **PCZTT** with a planar backbone demonstrated four times higher mobility than that of **PCZT** with a twisted backbone (Table 2). Further improvements of the mobilities would be possible by the combination with other prominent building blocks to enhance the intramolecular CT character and thin film crystallinity.[63]

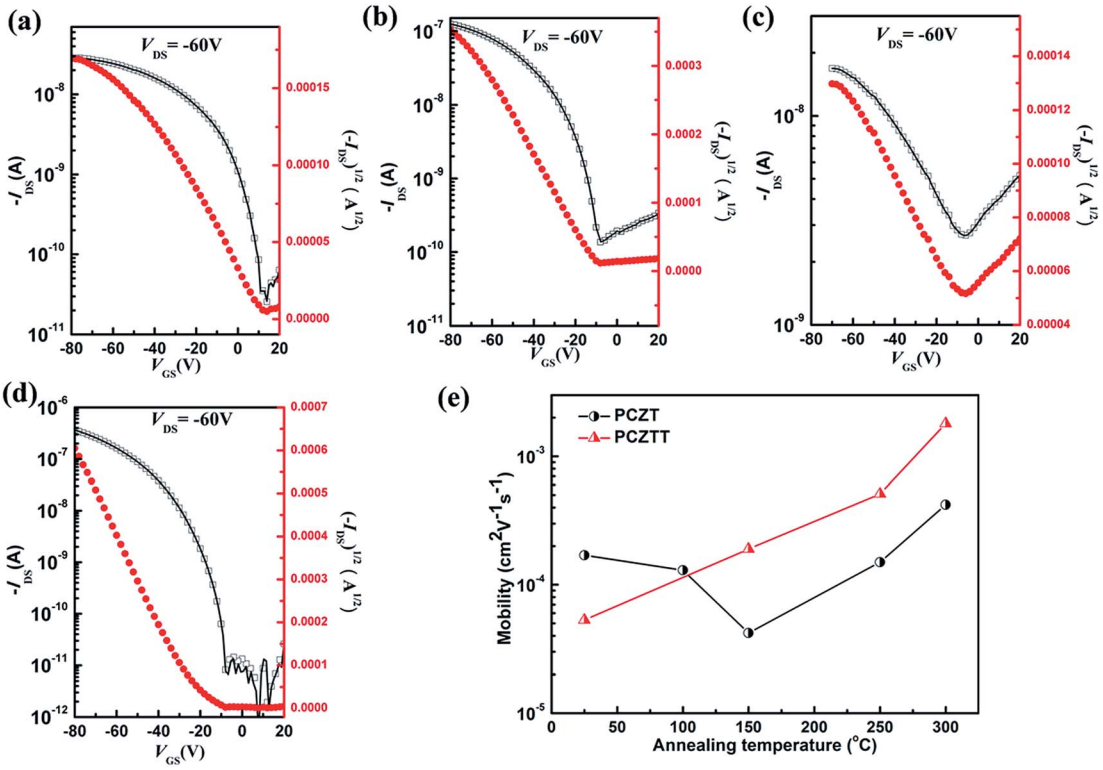

Fig. 4 Transfer characteristics of TFTs based on the thin films of (a) **PCZT** without annealing; (b) **PCZT** annealed at the optimized temperature of 300 °C; (c) **PCZTT** without annealing; (d) **PCZTT** annealed at the optimized temperature of 300 °C (L = 100 μm and W = 1 mm. All the measurements were done under ambient conditions). (e) Effects of annealing temperatures on the hole mobilities of **PCZT** and **PCZTT**.

Table 2 Summary of TFT device performances

Sample/annealing temp.	μ_h [μ_{h_max}][a] ($cm^2\ V^{-1}\ s^{-1}$)	V_{th} (V)	I_{on}/I_{off}
PCZT (N/A)	1.4×10^{-4} [1.7×10^{-4}]	13	10^2–10^3
100 °C	1.1×10^{-4} [1.3×10^{-4}]	−6	10^2–10^3
150 °C	3.5×10^{-5} [4.2×10^{-5}]	−10	10^2–10^3
250 °C	1.4×10^{-4} [1.5×10^{-4}]	−8	10^2–10^3
300 °C	**3.0×10^{-4} [4.2×10^{-4}]**	−8	10^2–10^3
PCZTT (N/A)	5.1×10^{-5} [5.3×10^{-5}]	−7	10^1–10^2
150 °C	1.8×10^{-4} [1.9×10^{-4}]	−15	10^2–10^3
250 °C	4.8×10^{-4} [5.1×10^{-4}]	−30	10^2–10^3
300 °C	**1.4×10^{-3} [1.8×10^{-3}]**	−6	10^5–10^6

[a] Mobility values are measured in air. The mobilities under optimized annealing conditions are indicated in boldface. The average values are calculated over 3 devices and the highest values are listed in parentheses.

Characterization of molecular organization and film morphologies

Although the TFT performances of the **CZ**-based polymers were somewhat correlated with their HOMO levels (**PCZTT** has a shallower HOMO level and higher μ_h than **PCZT**), it is necessary to investigate the organization of the thin films by GIWAXS measurements. The 2D-GIWAXS patterns provided information about the molecular packing structures (Fig. 5). The corresponding 1D profiles are shown in Fig. S7.† The pristine thin film of **PCZT** displayed very weak reflections (Fig. 5a and S7a†). Only after thermal annealing at 300 °C, one could observe a primary reflection peak (100) located at $2\theta = 4.0°$ along the q_{xy} direction (in-plane direction). In addition, a reflection peak (010) located at $2\theta = 25.7°$ along the q_z direction (out-of-plane) was found in its 1D profile (Fig. S7b†). This result indicated that **PCZT** tends to adopt a face-on backbone packing orientation with the chain-to-chain and π–π stacking distances of 22.0 Å and 3.5 Å, respectively (Fig. S8a†).[13,25] On the other hand, the thin film of **PCZTT** exhibited a primary diffraction peak (100) located at $2\theta = 4.9°$ along the q_z direction (out-of-plane) with a chain-to-chain packing distance of 18.0 Å (Fig. 5c and S7c†). This result suggested that **PCZTT** tends to adopt an edge-on backbone packing orientation (Fig. S8b†). Furthermore, the thermal annealing treatment at 300 °C explicitly intensified the primary diffraction peak (Fig. 5d and S7d†). Therefore, the higher mobility of **PCZTT** was reasonably attributed to its edge-on backbone packing orientations toward the Si substrate, which was favorable for the in-plane charge transport in the TFT devices (Fig. S8b†).[10,13,14,22,25] Overall, the GIWAXS results were well correlated with the TFT performances, and it was revealed that the polymers with a planar backbone show a better charge carrier transport property than those with a twist backbone.[10,11,13,22,25]

To elucidate the thermal annealing effects on the thin film quality, the surface morphology of the thin films was investigated using tapping-mode atomic force microscopy (AFM).[13,14] As shown in Fig. 6, the thin films of **PCZT** showed a relatively amorphous morphology. A root-mean-square (RMS) roughness

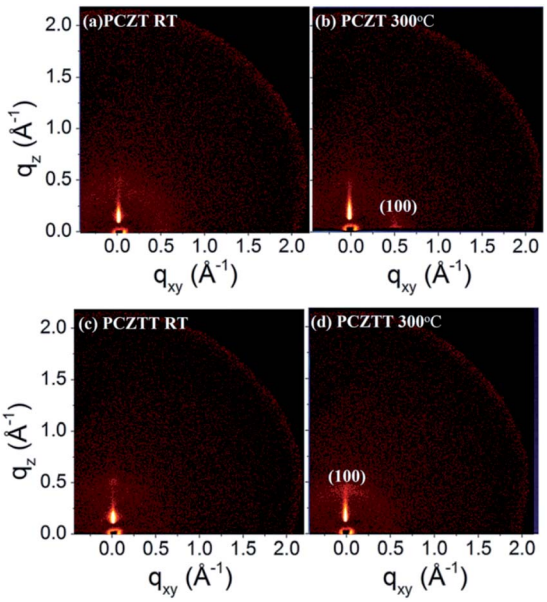

Fig. 5 GIWAXS patterns of the thin films at different annealing temperatures. **PCZT**: (a) RT and (b) 300 °C; **PCZTT**: (c) RT and (d) 300 °C.

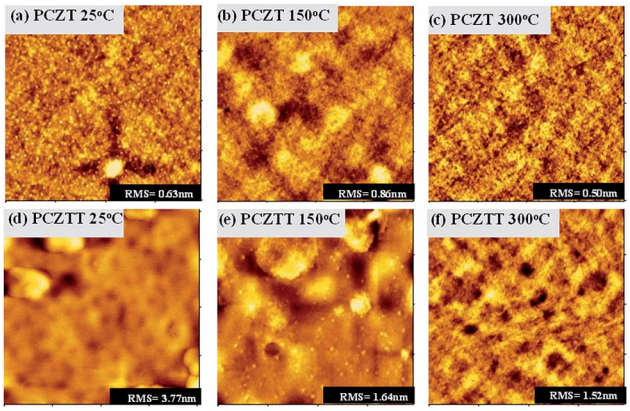

Fig. 6 Tapping-mode AFM topography images of the thin films of (a to c) **PCZT** and (d to f) **PCZTT**, prepared by thermal annealing at different temperatures. Annealing temperatures (for 10 min) are depicted in each image. AFM size: 2 × 2 μm^2.

of 0.63 nm was observed for the pristine film (Fig. 6a). Thermal annealing at 150 °C increased the RMS value to 0.86 nm, whereas it decreased to 0.50 nm at the thermal annealing temperature of 300 °C (Fig. 6b and c). A smoother surface morphology would result in a better interfacial contact with the Au electrode, and accordingly, the charge carrier transport would be facilitated.[14,22,25] Therefore, the thin film annealed at 150 °C showed the lowest mobility, while annealing at 300 °C led to the highest mobility in the case of **PCZT**. On the other hand, the RMS values of the **PCZTT** linearly decreased as the thermal annealing temperature increased. For instance, the pristine film showed a relatively rough surface morphology (RMS = 3.77 nm) with some small "holes" and aggregates,

indicating an inferior interconnectivity and a low quality thin film (Fig. 6d). In contrast, much smoother surface morphologies (RMS = 1.52–1.64 nm) with the interconnected grains were obtained after thermal annealing at 150–300 °C (Fig. 6e and f). As a consequence, largely interconnected grains would facilitate the charge carrier transport of the **PCZTT**-based TFTs.[14,22,25] Overall, the results were consistent with the observed changes in μ_h upon thermal annealing.

Conclusion

In summary, a new linear-type dibromocarbazoledioxazine derivative was synthesized and fully characterized. By using this building block as a bifunctional monomer, two **CZ**-based semiconducting polymers, namely **PCZT** and **PCZTT**, were, for the first time, synthesized by Stille polycondensation. The LUMO levels of both polymers were almost the same due to the dominating electron-withdrawing effect of the **CZ** unit, while there were differences in the HOMO levels and backbone planarity. **PCZTT** possessed by 0.07 eV a shallower HOMO level and more planar backbone, producing a narrower band gap. The charge-transporting properties, estimated from the TFT performances, suggested that **PCZTT** showed a four times higher hole mobility than **PCZT**. In addition to the HOMO level, the enhanced hole mobility was due to the edge-on backbone packing orientations toward the Si substrate, originating from the stronger intermolecular interactions induced by the planar backbone of **PCZTT**. This study highlights the promising use of the **CZ**-based semiconductors in the field of organic electronics. It is also interesting to note that a subtle change in the spacer structure (thiophene *vs.* thienothiophene) dramatically alters the molecular packing orientations and TFT performances. Further improvements of the **CZ**-based organic semiconductors by backbone and side chain engineering are currently underway in our laboratory.

Conflicts of interest

There are no conflicts to declare.

Acknowledgements

This work was partially supported by the Heiwa Nakajima Foundation, the Ogasawara Foundation for the Promotion of Science and Engineering, the Yazaki Memorial Foundation for Science and Technology, and the Support for Tokyotech Advanced Researchers. The authors thank Mr Hiroshi Iida and Mr Masato Koizumi (Center for Advanced Materials Analysis, Tokyo Institute of Technology) for operating the GIWAXS instrument and MALDI-TOF mass spectrometer, respectively.

Notes and references

1 X. Li, H. Wang, J. A. Schneider, Z. Wei, W. Lai, W. Huang, F. Wudl and Y. Zheng, *J. Mater. Chem. C*, 2017, **5**, 2781–2785.
2 Y. Cai, X. Zhang, X. Xue, D. Wei, L. Huo and Y. Sun, *J. Mater. Chem. C*, 2017, **5**, 7777–7783.
3 Y. Wang, Y. Liu, S. Chen, R. Peng and Z. Ge, *Chem. Mater.*, 2013, **25**, 3196–3204.
4 Y. Wang, F. Yang, Y. Liu, R. Peng, S. Chen and Z. Ge, *Macromolecules*, 2013, **46**, 1368–1375.
5 Y. Wang, M. F. G. Klein, J. Hiyoshi, S. Kawauchi, W. W. H. Wong and T. Michinobu, *J. Photopolym. Sci. Technol.*, 2015, **28**, 385–391.
6 Y. Liu, Y. Wang, L. Ai, Z. Liu, X. Ouyang and Z. Ge, *Dyes Pigm.*, 2013, **121**, 363–371.
7 W. Li, M. Otsuka, T. Kato, Y. Wang, T. Mori and T. Michinobu, *Beilstein J. Org. Chem.*, 2016, **12**, 1401–1409.
8 Q. Liu, Y. Liu, Y. Wang, L. Ai, X. Ouyang, L. Han and Z. Ge, *New J. Chem.*, 2013, **37**, 3627–3633.
9 W. Wu, J. Li, Z. Zhao, X. Yang and X. Gao, *Org. Chem. Front.*, 2017, **4**, 823–827.
10 Y. Wang, H. Masunaga, T. Hikima, H. Matsumoto, T. Mori and T. Michinobu, *Macromolecules*, 2015, **48**, 4012–4023.
11 Y. Wang, M. Nakano, T. Michinobu, Y. Kiyota, T. Mori and K. Takimiya, *Macromolecules*, 2017, **50**, 857–864.
12 Y.-Y. Lai, H.-H. Chang, Y.-Y. Lai, W.-W. Liang, C.-E. Tsai and Y.-J. Cheng, *Macromolecules*, 2015, **48**, 6994–7006.
13 Y. Wang, T. Kadoya, L. Wang, T. Hayakawa, M. Tokita, T. Mori and T. Michinobu, *J. Mater. Chem. C*, 2015, **3**, 1196–1207.
14 H. Li, F. Liu, X. Wang, C. Gu, P. Wang and H. Fu, *Macromolecules*, 2013, **46**, 9211–9219.
15 Y. Wang, R. Hosokawa, T. Mori and T. Michinobu, *Bull. Chem. Soc. Jpn.*, 2017, **90**, 1041–1049.
16 I. Osaka, M. Akita, T. Koganezawa and K. Takimiya, *Chem. Mater.*, 2012, **24**, 1235–1243.
17 M. Akita, I. Osaka and K. Takimiya, *Materials*, 2013, **6**, 1061–1071.
18 K. Kawabata, M. Saito, N. Takemura, I. Osaka and K. Takimiya, *Polym. J.*, 2017, **49**, 169–176.
19 M. S. White, M. Kaltenbrunner, E. D. Głowacki, K. Gutnichenko, G. Kettlgruber, I. Graz, S. Aazou, C. Ulbricht, D. A. M. Egbe, M. C. Miron, Z. Major, M. C. Scharber, T. Sekitani, T. Someya, S. Bauer and N. S. Sariciftci, *Nat. Photonics*, 2013, **7**, 812–816.
20 P. Heremans, A. K. Tripathi, A. de Jamblinne de Meux, E. C. P. Smits, B. Hou, G. Pourtois and G. H. Gelinck, *Adv. Mater.*, 2016, **28**, 4266–4282.
21 Y. Wang and T. Michinobu, *Bull. Chem. Soc. Jpn.*, 2017, **90**, 1388–1400.
22 Y. Wang, T. Hasegawa, H. Matsumoto, T. Mori and T. Michinobu, *Adv. Funct. Mater.*, 2017, **27**, 1604608.
23 G. Kim, S.-J. Kang, G. K. Dutta, Y.-K. Han, T. J. Shin, Y.-Y. Noh and C. A. Yang, *J. Am. Chem. Soc.*, 2014, **136**, 9477–9483.
24 H. Chen, Y. Guo, G. Yu, Y. Zhao, J. Zhang, D. Gao, H. Liu and Y. Liu, *Adv. Mater.*, 2012, **24**, 4618–4622.
25 Y. Wang, A. T. Tan, T. Mori and T. Michinobu, *J. Mater. Chem. C*, 2018, DOI: 10.1039/C7TC04993E.
26 Y. Wang and T. Michinobu, *J. Mater. Chem. C*, 2016, **4**, 6200–6214.
27 F. S. Melkonyan, W. Zhao, M. Drees, N. D. Eastham, M. J. Leonardi, M. R. Butler, Z. Chen, X. Yu,

R. P. H. Chang and M. A. Ratner, *J. Am. Chem. Soc.*, 2016, **138**, 6944–6947.
28 J.-H. Kim, S. A. Shin, J. B. Park, C. E. Song, W. S. Shin, H. Yang, Y. Li and D.-H. Hwang, *Macromolecules*, 2014, **47**, 1613–1622.
29 I. Osaka, Y. Houchin, M. Yamashita, T. Kakara, N. Takemura, T. Koganezawa and K. Takimiya, *Macromolecules*, 2014, **47**, 3502–3510.
30 H. S. Kim, G. Huseynova, Y.-Y. Noh and D.-H. Hwang, *Macromolecules*, 2017, **50**, 7550–7558.
31 C. Wang, H. Dong, W. Hu, Y. Liu and D. Zhu, *Chem. Rev.*, 2011, **112**, 2208–2267.
32 Y. Zhao, Y. Guo and Y. Liu, *Adv. Mater.*, 2013, **25**, 5372–5391.
33 W. Li, K. H. Hendriks, M. M. Wienk and R. A. J. Janssen, *Acc. Chem. Res.*, 2016, **49**, 78–85.
34 T. Lei, J.-Y. Wang and J. Pei, *Acc. Chem. Res.*, 2014, **47**, 1117–1126.
35 W. Jiang, Y. Li and Z. Wang, *Acc. Chem. Res.*, 2014, **47**, 3135–3147.
36 N. Liang, K. Sun, Z. Zheng, H. Yao, G. Gao, X. Meng, Z. Wang, W. Ma and J. Hou, *Adv. Energy Mater.*, 2016, **6**, 1600060.
37 Z. Wu, C. Sun, S. Dong, X.-F. Jiang, S. Wu, H. Wu, H.-L. Yip, F. Huang and Y. Cao, *J. Am. Chem. Soc.*, 2016, **138**, 2004–2013.
38 M. Gsänger, D. Bialas, L. Huang, M. Stolte and F. Würthner, *Adv. Mater.*, 2016, **28**, 3615–3645.
39 N. C. Debnath and S. A. Vaidya, *Prog. Org. Coat.*, 2006, **56**, 159–168.
40 P. T. C. Lee, C.-W. Chiu, T.-M. Lee, T.-Y. Chang, M.-T. Wu, W.-Y. Cheng, S.-W. Kuo and J.-J. Lin, *ACS Appl. Mater. Interfaces*, 2013, **5**, 5914–5920.
41 P. T. C. Lee, C.-W. Chiu, L.-Y. Chang, P.-Y. Chou, T.-M. Lee, T.-Y. Chang, M.-T. Wu, W.-Y. Cheng, S.-W. Kuo and J.-J. Lin, *ACS Appl. Mater. Interfaces*, 2014, **6**, 14345–14352.
42 M. Buccella, A. Dorigato, F. Crugnola, M. Caldara and L. Fambri, *J. Appl. Polym. Sci.*, 2015, **132**, 41452.
43 W. Zhang, J. Wang, J. Mao, L. Hu, X. Wu and C. Guo, *Tetrahedron Lett.*, 2016, **57**, 1985–1989.
44 A. Kimoto and Y. Tajima, *Org. Lett.*, 2012, **14**, 2282–2285.
45 M. Ikeda, K. Kitahara and H. Nishi, *J. Heterocycl. Chem.*, 1990, **27**, 1575–1579.
46 M. Ikeda, K. Kitahara and H. Nishi, *J. Heterocycl. Chem.*, 1991, **28**, 1165–1171.
47 M. Ikeda, K. Kitahara, H. Nishi, H. Nakahara and K. Fukuda, *Chem. Lett.*, 1991, **20**, 1177–1180.
48 M. Ikeda, K. Kitahara and H. Nishi, *J. Heterocycl. Chem.*, 1992, **29**, 289–294.
49 H. Tatsumi, Y. Wang, Y. Aizawa, M. Tokita, T. Mori and T. Michinobu, *J. Phys. Chem. C*, 2016, **120**, 26686–26694.
50 N. Blouin and M. Leclerc, *Acc. Chem. Res.*, 2008, **41**, 1110–1119.
51 S. Wakim, S. Beaupré, N. Blouin, B. Aich, S. Rodman, R. Gaudiana, Y. Tao and M. Leclerc, *J. Mater. Chem.*, 2009, **19**, 5351–5358.
52 S. H. Park, A. Roy, S. Beaupré, S. Cho, N. Coates, J. S. Moon, D. Moses, M. Leclerc, K. Lee and A. J. Heeger, *Nat. Photonics*, 2009, **3**, 297–302.
53 S. Beaupré and M. Leclerc, *J. Mater. Chem. A*, 2013, **1**, 11097–11105.
54 N. Blouin, M. Leclerc, B. Vercelli, S. Zecchin and G. Zotti, *Macromol. Chem. Phys.*, 2006, **207**, 175–182.
55 N. Blouin, A. Michaud, S. Wakim, P.-L. T. Boudreault, M. Leclerc, B. Vercelli, S. Zecchin and G. Zotti, *Macromol. Chem. Phys.*, 2006, **207**, 166–174.
56 J. Lu, F. Liang, N. Drolet, J. Ding, Y. Tao and R. Movileanua, *Chem. Commun.*, 2008, 5315–5317.
57 S. Cai, L. Chen, D. Zha and Y. A. Chen, *J. Polym. Sci., Part A: Polym. Chem.*, 2013, **51**, 624–634.
58 S. Habuchi, H. Fujita, T. Michinobu and M. Vacha, *J. Phys. Chem. B*, 2011, **115**, 14404–14415.
59 H. Piwoński, T. Michinobu and S. Habuchi, *Nat. Commun.*, 2017, **8**, 15256.
60 J. W. Choi, C. Kulshreshtha, G. P. Kennedy, J. H. Kwon, S. Jung and M. Chae, *Sol. Energy Mater. Sol. Cells*, 2011, **95**, 2069–2076.
61 Y. Wang, T. Hasegawa, H. Matsumoto, T. Mori and T. Michinobu, *Adv. Mater.*, 2018, DOI: 10.1002/adma.201707164.
62 N. S. Baek, S. K. Hau, H.-L. Yip, O. Acton, K.-S. Chen and A. K.-Y. Jen, *Chem. Mater.*, 2008, **20**, 5734–5736.
63 Y. Wang, T. Hasegawa, H. Matsumoto, T. Mori and T. Michinobu, *Adv. Funct. Mater.*, 2017, **27**, 1701486.

